Environmental Science & Technology

pubs.acs.org/est

Article

Elucidating the Trade-off between Membrane Wetting Resistance and Water Vapor Flux in Membrane Distillation

Chenxi Li, Xuesong Li,* Xuewei Du, Ying Zhang, Wei Wang, Tiezheng Tong, Arun Kumar Kota, and Jongho Lee*

Cite This: *Environ. Sci. Technol.* 2020, 54, 10333−10341

Read Online

ACCESS | Metrics & More | Article Recommendations | Supporting Information

ABSTRACT: Membrane distillation (MD) has been receiving considerable attention as a promising technology for desalinating industrial wastewaters. While hydrophobic membranes are essential for the process, increasing membrane surface hydrophobicity generally leads to the reduction of water vapor flux. In this study, we investigate the mechanisms responsible for this trade-off relation in MD. We prepared hydrophobic membranes with different degrees of wetting resistance through coating quartz fiber membranes with a series of alkylsilane molecules while preserving the fiber structures. A trade-off between wetting resistance and water vapor flux was observed in direct-contact MD experiments, with the least-wetting-resistant membrane exhibiting twice as high vapor flux as the most wetting-resistant membrane. Electrochemical impedance analysis, combined with fluorescence microscopy, elucidated that a lower wetting resistance (still water-repelling) allows deeper penetration of the liquid−air interfaces into the membrane, resulting in an increased interfacial area and therefore a larger evaporative vapor flux. Finally, we performed osmotic distillation experiments employing anodized alumina membranes that possess straight nanopores with different degrees of wetting resistance, observed no trade-off, and substantiated this proposed mechanism. Our study provides a guideline to tailor the membrane surface wettability to ensure stable MD operations while maximizing the water recovery rate.

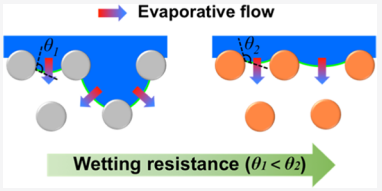

INTRODUCTION

Consuming approximately 20% of global freshwater withdrawal, industrial sector is the second largest consumer of freshwater resources following the agriculture sector.[1] Its rapidly growing freshwater consumption makes water reclamation from industrial wastewaters an important practice in reducing the freshwater demand.[2] Moreover, the increasingly stringent discharge regulation such as zero liquid discharge also necessitates efficient water reclamation and reuse from industrial wastewaters.[3] A significant fraction of industrial wastewaters such as those generated from manufacturing, mining, oil, and gas sectors,[4] typically contains a variety of contaminants including highly concentrated salts (up to 360 000 mg L^{-1}), oil, alcohols, and other organic pollutants.[2,5] As a state-of-the-art membrane separation technology for recovering clean water from industrial wastewaters, reverse osmosis (RO), however, has a treatable salinity limit (<~70 000 mg L^{-1}) due to the prohibitively high osmotic pressure to overcome and exhibits unsatisfactory rejection against some specific organic pollutants.[5,6]

Membrane distillation (MD) has attracted considerable attention in recent years as an alternative process for water reclamation from highly saline wastewaters.[7−12] MD is a thermal desalination process in which water vapor is driven by a vapor pressure gradient from a hot feed to a cold permeate across a porous hydrophobic membrane. The phase-change desalination mechanism makes its water flux and energy consumption fairly insensitive to the feed salinity and enables near-complete salt rejection. Like other thermal desalination processes, MD is an energy-intensive process. However, MD can be operated at a moderate temperature, much lower than the boiling point of water, which renders MD a potentially low-energy-cost process if low-grade heat or waste heat is utilized.[13]

In the MD process, the membrane must resist wetting to keep the feed and permeate separated.[14] However, ubiquitous low-surface-tension contaminants in industrial wastewaters, such as oil, alcohols, and surfactants, can increase the risk of membrane pore wetting in the MD operation.[10,15,16] As such, developing highly wetting-resistant membranes has been extensively investigated, commonly through modifying the membrane surface by grafting low-surface-energy materials and/or creating a re-entrant structure to the extent that the membrane becomes omniphobic (i.e., resisting low-surface-tension liquids).[17−22]

While those modified membranes exhibited excellent wetting resistance, a noticeable reduction in the MD water vapor flux has been observed in many experiments. Figure 1 shows a summary of MD water flux changes in recent publications (detailed data are shown in Table S1),[8−10,19,23−32]

Received: April 22, 2020
Revised: July 6, 2020
Accepted: July 23, 2020
Published: July 23, 2020

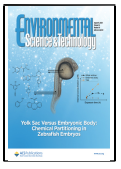

https://dx.doi.org/10.1021/acs.est.0c02547
Environ. Sci. Technol. 2020, 54, 10333−10341

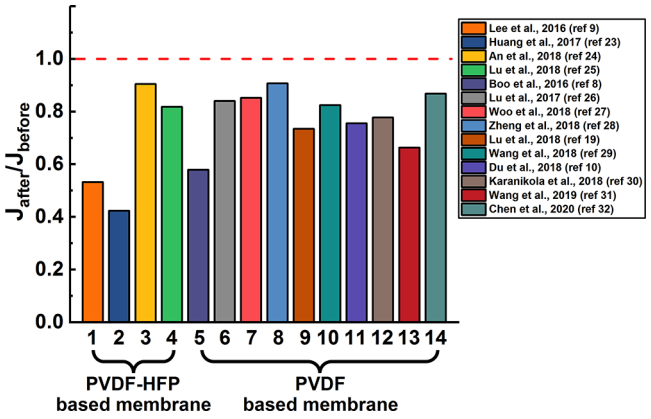

Figure 1. Ratios of water flux after the surface modification of PVDF- or PVDF-HFP-based membranes with low-surface-energy materials (J_{after}) to water flux before the modification (J_{before}), calculated from the data in the literature of direct-contact membrane distillation (DCMD). PVDF stands for poly(vinylidene fluoride) and PVDF-HFP stands for poly(vinylidene fluoride-*co*-hexafluoropropylene).

as a result of surface modifications of hydrophobic membranes made of poly(vinylidene fluoride) (PVDF) or poly(vinylidene fluoride-*co*-hexafluoropropylene) (PVDF-HFP) with low-surface-energy materials. Lower water vapor fluxes were observed after the modifications ($J_{after}/J_{before} < 1$) in all surveyed cases, although a few exceptions were also reported.[33−35] While MD water flux is significantly influenced by membrane structures,[13] detailed information on the change in thickness, porosity, and pore size after such modifications is rarely available in the literature (summarized in Table S1), making it difficult to examine the sole impact of wetting resistance on water flux.

In a very recent study, this trade-off relation between wetting resistance and water vapor flux has been investigated using PVDF-based membranes with different wettabilities.[31] It was suggested that a membrane with a lower wetting resistance (but still water-repelling) has a larger number of partially wetted pores, leading to a higher liquid−air interfacial area and thus a higher water vapor flux. While this hypothesis was supported by the numerical simulations of a dynamic liquid−air interface formation, further experimental verification is necessary to thoroughly substantiate and validate this hypothesis. In addition, while PVDF membranes of irregular structures were used in the study, the generalization of this hypothesis to other types of membranes warranties further investigation. Since an enhanced wetting resistance at the expense of water vapor flux may cause reduced efficiency of MD process for water reclamation, it is of great importance to elucidate the underlying mechanism of such a trade-off relation, which will be critical to guarantee a stable MD operation without compromising the water vapor flux.

In this work, we elucidate the underlying mechanism for the trade-off relation between the membrane wetting resistance and water vapor flux in MD. We modify a fibrous membrane with a series of low-surface-energy alkylsilane molecules to fabricate hydrophobic/omniphobic membranes that possess varying degrees of wetting resistance while maintaining identical membrane structures and morphologies. We confirm the trade-off relation in direct-contact membrane distillation (DCMD) experiments with the fabricated membranes. We examine the impact of membrane thermal conductance, air−gap distance in the membrane, and the liquid−air interfacial area on the water flux using various techniques including thermal conductivity measurement, fluorescence microscopy, and electrochemical impedance spectroscopy (EIS). Further, we perform osmotic distillation (OD) experiments using porous alumina membranes that comprise straight nanopores, which exhibit different wettabilities but possess identical liquid−air interfacial areas available for water evaporation and condensation. Taken together, we identify the determining factor for the trade-off relation and propose potential mechanisms. Our findings can serve as a guideline for membrane fabrications suitable for MD in various industrial applications.

MATERIALS AND METHODS

Materials and Chemicals. Quartz fiber (QF) membranes (membrane type: QR-100) with an average thickness of 0.38 mm were supplied by Sterlitech (WA). This type of QF membrane retains 99.99% of dioctylphthalate-derived particles having a diameter of 0.3 μm (data provided by the supplier) and the porosity of QR-100 is 79.3 ± 1.3% determined by the pycnometric method.[36] Nanoporous anodized aluminum oxide (AAO) membranes with a nominal diameter of 200 nm and porosity of approximately 10% were supplied by InRedox (CO). Four silane agents were selected for the surface silanization of QF membranes and AAO membranes: trimethoxy(propyl)silane (AS, 97%, Sigma-Aldrich), (3,3,3-trifluoropropyl)trimethoxysilane (FAS-3, 98%, Gelest Inc.), nonafluorohexyltriethoxysilane (FAS-9, 98%, Gelest Inc.), and 1*H*,1*H*,2*H*,2*H*-perfluorodecyltriethoxysilane (FAS-17, 98%, Gelest Inc.). *N*,*N*-Dimethylformamide (DMF, 99.8%) was purchased from VWR International. Hexadecane (≥98%), sodium chloride (NaCl, ≥99%), and sodium dodecyl sulfate (SDS) were obtained from Fisher Scientific. Distilled water was generated by a Synergy UV water purification system (Millipore, Billerica, MA). The other chemicals were supplied by Sigma-Aldrich unless otherwise stated.

Fabrication of Hydrophobic Membranes with Different Wetting Resistances. The hydrophobic modification processes of QF and AAO membranes were schematically illustrated in Figure S1. The pristine QF membrane was immersed in a DMF solution containing 3.5 wt % poly(vinylidene fluoride-*co*-hexafluoropropylene) (PVDF-HFP, $M_W \sim 400\,000$) and 1% v/v silane (i.e., AS, FAS-3, FAS-9, and FAS-17) for 2 h under continuous shaking, which was subsequently placed in an oven at 105 °C for 4 h to completely remove DMF. The modified QF membrane was subjected to a hot-press treatment under 0.5 bar at 160 °C for 1 h to enhance its compactness. The hydrophobic AAO membranes were fabricated by soaking the pristine membrane in a hexane solution containing 1% v/v silane (i.e., AS, FAS-3, FAS-9, and FAS-17) for 20 h, followed by a heat treatment at 105 °C for 4 h after a thorough rinse with hexane.

Membrane Characterizations. The surface morphologies and cross-sectional structures of modified membranes were characterized using a scanning electron microscope (SEM, FEI Quanta 650). The surface wettabilities were characterized by measuring the static contact angles of different liquids using a goniometer (Ramé-Hart 200-F1). Thermal conductivities of membranes were assessed using a thermal conductivity analyzer (Hot Disk TPS 2500S) equipped with a thin-film sensor with a nickel double spiral insulated in a thin layer of Kapton. For the thermal conductivity analysis, 20 membrane samples with the same size were stacked and placed on each

https://dx.doi.org/10.1021/acs.est.0c02547
Environ. Sci. Technol. 2020, 54, 10333−10341

side of the sensor, which were compressed under a fixed pressure (0.6 bar).

Silicon wafers were used to assess the surface energies of different silanes. Prior to the surface silanization, the silicon wafer was first cleaned with a piranha solution (3:1 v/v sulfuric acid: hydrogen peroxide mixture) for 2 h, followed by a thorough rinse with distilled water. After rinsing, the silicon wafer was dried at 105 °C for 2 h. The silanization of the cleaned silicon wafer was performed following the same protocol as that used for AAO membrane modification. The method proposed by Wu[37] was used to calculate the surface energy of a silane-modified surface as it is suitable for analyzing the surface with a relatively low surface energy.[38] The total surface energy (γ_{sv}) may be decomposed into dispersion (γ_{sv}^{d}) and polar components (γ_{sv}^{p})

$$\gamma_{sv} = \gamma_{sv}^{d} + \gamma_{sv}^{p} \quad (1)$$

By measuring the static contact angles of water (θ_{water}) and diiodomethane ($\theta_{D\text{-}M}$) on modified silicon wafers, γ_{sv}^{d} and γ_{sv}^{p} can be calculated using the following equations

$$[1 + \cos(\theta_{water})]\gamma_{water} = 4\left(\frac{\gamma_{water}^{d}\cdot\gamma_{sv}^{d}}{\gamma_{water}^{d} + \gamma_{sv}^{d}} + \frac{\gamma_{water}^{p}\cdot\gamma_{sv}^{p}}{\gamma_{water}^{p} + \gamma_{sv}^{p}}\right) \quad (2)$$

$$[1 + \cos(\theta_{D-M})]\gamma_{D-M} = 4\left(\frac{\gamma_{D-M}^{d}\cdot\gamma_{sv}^{d}}{\gamma_{D-M}^{d} + \gamma_{sv}^{d}} + \frac{\gamma_{D-M}^{p}\cdot\gamma_{sv}^{p}}{\gamma_{D-M}^{p} + \gamma_{sv}^{p}}\right) \quad (3)$$

The dispersive components of water (γ_{water}^{d}) and diiodomethane ($\gamma_{D\text{-}M}^{d}$) are 21.8 and 49.5 mN m^{-1}, respectively, while the polar components of water (γ_{water}^{p}) and diiodomethane ($\gamma_{D\text{-}M}^{d}$) are 51.0 and 1.3 mN m^{-1}, respectively.[39]

The protrusion of liquid−air interfaces into the membrane pores was assessed via electrochemical impedance spectroscopy (EIS). The modified QF membrane was mounted in a cross-flow membrane cell having an effective area of 3 cm^2 (12 mm × 25 mm). Each channel was filled with the electrolyte solution (1 M NaCl solution with different concentrations of SDS). A titanium sheet was inserted into each flow channel to directly contact the membrane, and the other end was connected to a potentiostat (Interface 1010E, Gamry Instruments) with built-in software to monitor the impedance of the system. The frequency was varied from 10^3 to 10^6 Hz. The detailed procedure to estimate the effective capacitance from EIS measurements is described in the Supporting Information, Section 1.

The degree of penetration of feed water into the membranes was visualized via fluorescence microscopy. The modified QF membrane was assembled in a dead-end filtration cell, which was filled with an aqueous solution containing 0.01 mg mL^{-1} Rhodamine B and 0.01 mM SDS ($\gamma \approx 66$ mN m^{-1}, the same surface tension as the feed water at 60 °C) for 0.5 h. The height of the liquid solution in the dead-end cell was 10 cm, and the hydraulic pressure applied on the membrane was approximately 1 kPa, simulating the hydraulic pressure in the feed channel of the membrane cell during DCMD tests. After staining, the membrane sample was trimmed with blades and visualized by an upright configuration wide-field microscope (Olympus BX53).

DCMD Experiments of Modified Membranes. Water vapor fluxes across the modified QF membranes were measured by a bench-scale DCMD unit with a cross-flow membrane cell with an effective membrane area of 15 cm^2 (60 mm × 25 mm). NaCl solution (0.5 M) at 60 °C and distilled water at 20 °C were used as the feed and permeate solutions, respectively, whose temperatures were maintained using two recirculating water baths (Polystat Standard, Cole-Parmer). The feed had a slightly higher cross-flow velocity (5.6 cm s^{-1}) than the permeate (3.7 cm s^{-1}), which caused a higher pressure in the feed side than in the permeate side and therefore allowed for an explicit detection of membrane pore wetting. Details on measuring the water vapor flux and salt rejection are described in the Supporting Information, Section 2 as well as in our previous publication.[20]

Osmotic Distillation (OD) Experiments of Modified Membranes. Water vapor fluxes across the modified AAO membranes under isothermal condition were assessed by a bench-scale OD setup used in our previous studies.[40,41] The OD setup comprises two chambers that were filled with deionized water (feed) and 4 M NaCl solution (draw), respectively, with the silane-modified AAO membrane mounted in between. The effective membrane area was 28.3 mm^2 (diameter is 6 mm). The temperature of the entire OD setup was kept constant at 40 °C using a water jacket circulated from an external temperature-controlled water bath (Polystat Standard, Cole-Parmer). Magnetic stir bars were used to facilitate the mixing of liquid bulk and minimize concentration polarization.

The conductivity of the feed solution was monitored using a conductivity probe (isoPod, eDaq, CO) and a Matlab-coded program to detect salt leakage. The volume change of the draw solution was determined through a glass syringe (Hamilton Company, NV, USA, 250 μL volume, the accuracy of ± 2.5 μL) that was connected to the draw solution chamber. The water flux, J_w (L m^{-2} h^{-1}), through the membrane was calculated from the rate of volume change of water in the syringe.

RESULTS AND DISCUSSION

Enhancing Wetting Resistance of Hydrophobic Membranes Leads to a Lower Water Vapor Flux in DCMD. Investigating the impact of surface wettability on water vapor flux in DCMD requires us to fabricate a series of membranes with different surface wettabilities but having nearly identical membrane structures. Accordingly, all pristine QF membranes were modified following the same protocol except the type of silane molecules used. SEM micrographs in Figure 2a,b depict the surface morphology of two QF membranes modified with AS (AS QF membrane) and FAS-17 (FAS-17 QF membrane), respectively. SEM images of other modified QF membranes are also available in Figure S2. The resembled structures and similar fiber diameter distributions in modified membranes suggest that the modification with PVDF-HFP/silanes had little effect on the structure of the QF membrane. The variations of thickness, pore size, and porosity in all modified QF membranes were also insignificant (Table S2).

The different carbon chain lengths and fluorine contents of the four silanes impart the QF membranes with different degrees of hydrophobicity. We used the method proposed by Wu[37] to estimate the surface energies of atomically smooth silicon wafers, which were coated with the four silanes (Figure 2c). As expected, the estimated surface energy decreases in the order of AS, FAS-3, FAS-9, and FAS-17 modified silicon

https://dx.doi.org/10.1021/acs.est.0c02547
Environ. Sci. Technol. 2020, 54, 10333−10341

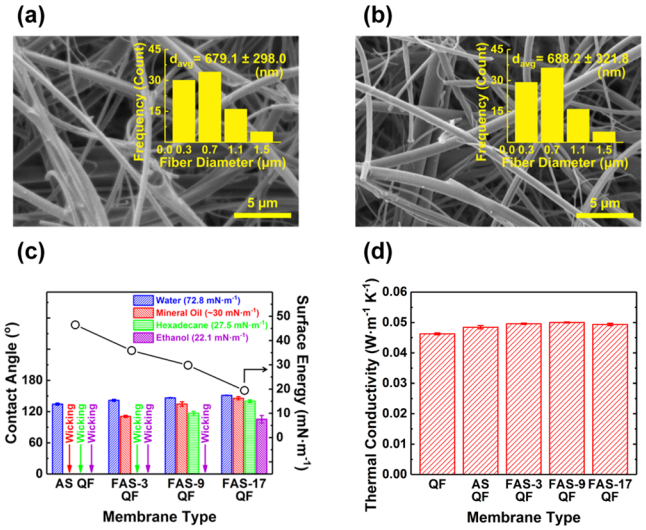

Figure 2. Characteristics of pristine and modified quartz fiber (QF) membranes. SEM micrographs of the morphologies of (a) AS QF and (b) FAS-17 QF membranes. The insets are fiber diameter distributions for each membrane sample. The average diameters (d_{avg}) of fibers in AS QF and FAS-17 QF membranes are 679.1 ± 298.0 and 688.2 ± 321.8 nm, respectively. (c) Static contact angles of four different testing liquids (water, mineral oil, hexadecane, and ethanol) on the surface of the AS QF, FAS-3 QF, FAS-9 QF, and FAS-17 QF membranes (bar chart). Black circles show the surface energies of the silane-modified silicon wafer surfaces, calculated from eqs 1 to 3. "Wicking" means that the membrane was wetted by testing liquid droplet, and no stable contact angle could be acquired. Error bars represent the standard deviations from three different membrane samples (both left and right contact angles were measured on each sample). (d) Thermal conductivities of the pristine QF membrane and modified QF membranes. Error bars represent the standard deviations from at least five measurements.

wafers, and these values agree well with the previously reported values in the literature.[39] The wettabilities of the modified QF membranes were assessed by measuring the static contact angles of several liquids having different surface tensions (γ): water (γ = 72.8 mN m^{-1}), mineral oil (~30 mN m^{-1}), hexadecane (27.5 mN m^{-1}), and ethanol (22.1 mN m^{-1}). All modified QF membranes exhibited water contact angles greater than 130°, indicating appropriate surface hydrophobicity for MD (Figure 2c). However, the membrane modified with a lower-surface-energy silane retained a lower-surface-tension liquid on its surface without being wetted. In two extreme cases, the FAS-17 QF membrane retained the all testing liquids and exhibited the highest liquid entry pressure (Table S2), while the AS QF membrane only repelled water (the lowest liquid entry pressure, Table S2) and was readily wetted by organic liquids.

Water vapor flux in MD is substantially impacted by the thermal conductivity of the membrane.[14] A low thermal conductivity is desired for MD to establish a steep temperature gradient across the membrane and therefore provides a large driving force for water vapor transport. We measured the thermal conductivities of the four differently modified QF membranes using a thermal conductivity meter. Likely due to the negligible mass fraction of coated silanes to the QF substrate, the measured thermal conductivities for all the membranes have very similar values (Figure 2d, ~0.05 W m^{-1} K^{-1}), from which we anticipate that the thermal conductivity would have little impact on the water vapor flux in our DCMD experiments.

The water vapor fluxes for the four differently modified QF membranes were measured in a lab-scale DCMD setup. Figure 3a shows the time traces of water flux and salt rejection of the

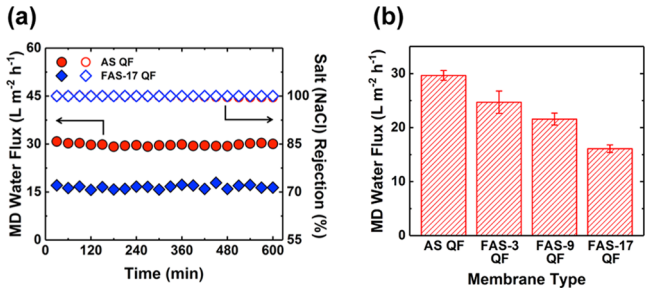

Figure 3. DCMD performance of modified QF membranes. (a) Water vapor flux and salt rejection of the AS QF (circle symbols) and FAS-17 QF (diamond symbols) membranes in DCMD tests. (b) DCMD water vapor fluxes of AS QF, FAS-3 QF, FAS-9 QF, and FAS-17 QF membranes. Error bars represent the standard deviations from three different membrane samples. All DCMD tests were conducted using 0.5 M NaCl at 60 °C as the feed solution and distilled water at 20 °C as the permeate solution.

AS QF and FAS-17 QF membranes. Time traces of water fluxes of all four membranes are available in Figure S3. Here, 0.5 M NaCl solution (60 °C) was used as a feed and distilled water (20 °C) as a permeate. Both membranes maintained stable water fluxes and nearly perfect salt rejections (>99%) over 10 h tests. Noticeably, the water vapor flux of AS QF membrane was approximately 30 L m^{-2} h^{-1}, nearly twice as high as that of the FAS-17 QF membrane. Combined with the FAS-3 QF and FAS-9 QF membranes, also with the nearly perfect salt rejections, a monotonic decrease in the water vapor flux was observed as the wetting resistance of the modified QF membrane increases (Figure 3b). Since all modified QF membranes exhibited similar membrane structures and thermal conductivities (Figure 2), we exclude the possibility that this trend in water flux was caused by any alteration of membrane structures or thermal properties. As such, our results corroborate the previously observed trade-off between membrane wetting resistance and water vapor flux in the MD process.[31] This observation directs us to investigate the mechanism, as explored in the following sections.

Membrane with a Higher Wetting Resistance Has a Smaller Liquid−Air Interfacial Area. Assuming identical membrane structures and thermal conductivities, supported by the previous results, the different water vapor fluxes in DCMD tests may be attributed to potential differences in (1) liquid−air interfacial areas available for evaporation and condensation and/or (2) the actual gap distance between the two membrane−solution interfaces across the membrane (i.e., effective membrane thickness). We first applied EIS to examine the differences in these two attributes of the modified QF membranes used in the DCMD process. EIS has been recently implemented to probe the wetting state of the hydrophobic membranes in the MD process.[42] Placed between electrolyte solutions (1 M NaCl), a hydrophobic membrane with trapped air may be modeled as a parallel circuit of a resistor and a capacitor when measuring its electrical impedance (Figure 4a).[42] The high ionic strength of the electrolyte solutions renders the solution impedance negligibly small compared to

https://dx.doi.org/10.1021/acs.est.0c02547
Environ. Sci. Technol. 2020, 54, 10333−10341

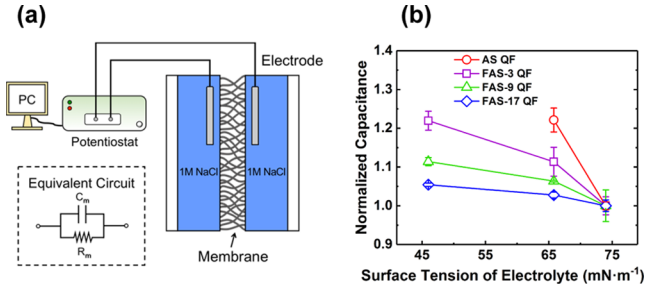

Figure 4. (a) Schematic illustration of the EIS system used for measuring the impedance of modified QF membranes. (b) Capacitances of the modified QF membranes estimated from the impedance measurements using 1 M NaCl solution with different surface tensions (SDS added) as the electrolyte solution. For each membrane sample, the capacitances were normalized to that with 1 M NaCl with no-added SDS. Error bars represent the standard deviations from three different membrane samples.

the membrane impedance (Figure S4). Therefore, we attribute the measured impedance to the membrane only. Based on this simple resistor−capacitor circuit model, we determined the equivalent capacitance of the air-filled hydrophobic membrane via EIS, which is correlated with the liquid−air interfacial area and effective membrane thickness.[42,43] Taking an air-filled hydrophobic membrane enclosed by the electrolyte as an ideal capacitor, its capacitance can be expressed as:[44]

$$C = \varepsilon_o \varepsilon_m \frac{A_{eff}}{d_{eff}} \quad (4)$$

where ε_o is the permittivity of air (or vacuum) and ε_m is the relative permittivity of the membrane−air matrix. The value of ε_m can be estimated by assuming the matrix as a homogeneous composite material of silica and air, but we obviate the need to calculate ε_m by normalizing the capacitances to a reference value (Figure 4b). A_{eff} is the effective liquid−air interfacial area and d_{eff} is the effective thickness of the unwetted membrane (i.e., the distance between two liquid−air interfaces). A detailed procedure for estimating the capacitance from EIS is available in the Supporting Information, Section 1.

If membrane pores are partially wetted, the penetration of the solution into pores can increase the liquid−air interfacial area (A_{eff}) and/or decrease the effective membrane thickness (d_{eff}), resulting in an increased capacitance (C). If the membrane pores are fully wetted, the membrane is equivalent to a resistor with negligible resistance, which can essentially be represented as a short circuit, leading to a drastically reduced overall impedance (Figure S4).

In our DCMD tests, the feed (0.5 M NaCl solution) temperature was 60 °C at which its surface tension becomes ~66 mN m^{-1}, lower than that of water at 25 °C (72 mN m^{-1}).[45] To simulate this reduced surface tension of the feed in our EIS measurement, we added the surfactant (sodium dodecyl sulfate, SDS) into the electrolyte (1 M NaCl solution) to reduce its surface tension to 66 mN m^{-1} and also to 46 mN m^{-1}. The Bode plots indicated that all modified QF membranes were in a nonwetted or partially wetted state during EIS measurements, except that the AS QF membrane was fully wetted and therefore the measurement was not possible when the surface tension of the electrolyte was reduced to 46 mN m^{-1} (Figure S4). When measured with a surfactant-free electrolyte, the FAS-17 QF membrane showed a much lower capacitance than the other membranes (Figure S5), probably because its exceptionally high water repellency does not allow the electrolyte to be in contact with the membrane surface and prevents the penetration of liquid into membrane pores.

Figure 4b shows the normalized capacitances of modified QF membranes after progressively adding SDS into the electrolyte. Reducing the surface tension of electrolyte is well-correlated with an increase in the equivalent capacitances for all modified membranes, suggesting that the membrane exposed to a lower-surface-tension liquid attains a higher liquid−air interfacial area or a lower effective membrane thickness, or both, which we attribute to the progression of the liquid−air interface into membrane pores. The interface progression into the membrane pores seems to be more prominent for the membrane having a lower wetting resistance, congruent with the higher increment of capacitance for the less wetting-resistant membrane.

Next, we employed fluorescence microscopy to investigate the penetration of liquid into the membrane. We selected FAS-9 QF and AS QF membranes due to their distinctly different wettabilities. The top surfaces of both membranes were stained by an aqueous solution containing 0.01 mg mL^{-1} Rhodamine B and 0.01 mM SDS under a hydraulic pressure of 1 kPa, simulating the feed surface tension ($\gamma \approx 66$ mN m^{-1}) and the hydraulic pressure applied on the membrane in our DCMD experiments.

Figure 5 visualizes the extent of the penetration of the aqueous dye into the two membranes. The thin bright strips

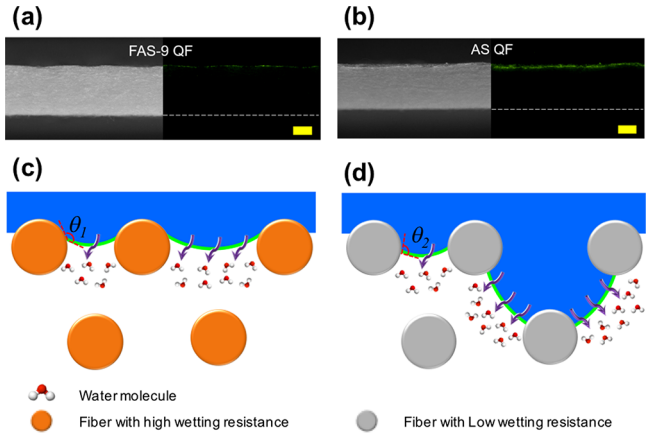

Figure 5. Optical (left) and fluorescence (right) microscopy images of the cross sections of (a) FAS-9 QF membrane and (b) AS QF membrane after the top surfaces of membranes were brought in contact with Rhodamine B solution with 0.01 mM SDS ($\gamma \approx 66$ mN m^{-1}). The green strips in the fluorescence microscopy images visualize the penetration depth of the solution into the membrane. The scale bar is 200 μm. Schematics (not drawn to scale) of membrane cross sections illustrating the degree of the liquid−air interface penetration and the liquid−air interfacial areas for fiber surfaces exhibiting (c) a high wetting resistance and (d) a low wetting resistance. θ is the local contact angle formed between the fiber surface and the liquid−air interface ($\theta_1 > \theta_2$).

observed on the upper edge of both membranes qualitatively showed that the liquid−air interface did not penetrate into the membrane, which implies that the gap distance between the two interfaces remained to be the membrane thickness during the DCMD experiments for both membranes. The observed maximum strip thickness of AS QF membrane (~30 μm) was

https://dx.doi.org/10.1021/acs.est.0c02547
Environ. Sci. Technol. 2020, 54, 10333−10341

greater than that of the FAS-9 QF membrane (~10 μm). Even these maximum thicknesses of the dye strips only accounted for a very small fraction of the entire membrane thickness (less than 6% even for AS QF membrane). The effective thickness (the thickness of the nonwetted part) of the AS QF membrane was only approximately 4% lower than that of the FAS-9 QF membrane. This difference is substantially smaller than the difference between the equivalent capacitances (15%) for AS QF and FAS-9 QF membranes, which were determined using EIS with the electrolyte of surface tension of 66 mN m^{-1} (Figure 4b). Since the equivalent capacitance can be expressed using the interfacial area (A_{eff}) and effective thickness (d_{eff}), given a certain type of membrane (eq 4), we conclude that the trade-off between wetting resistance and water vapor flux (Figure 3b) mainly stems from the differences of the liquid−air interfacial area.

Figure 5c,d illustrates potential mechanisms on how the liquid−air interfacial area can be changed by membrane wettability. For the membrane having a high wetting resistance (Figure 5c), the intrinsically high contact angle at the cylindrical fiber surface prevents water from penetrating into the membrane pores. The cross section of cylindrical fibers features a re-entrant curvature structure. Therefore, when the wetting resistance is reduced, the fiber network allows a liquid−air interface to be formed at the bottom side of the fibers to maximize the surface tension forces that resist the wetting front progression.[39,46,47] The formation of sagging liquid−air interfaces, in particular for fibers with a large interspacing, can induce the contact of the interface to the fiber surface in the subsequent layer, which results in a larger liquid−air interfacial area available for water evaporation and thereby allows for a higher water vapor flux (Figure 5d). This illustration is congruent with the larger thickness of the fluorescence dye layer (Figure 5a,b) and the greater dependency of the effective capacitance change on the surface tension for the less wetting-resistant membrane (Figure 4b).

We note that a more penetration of liquid into the membrane pores can cause a more severe temperature polarization and lead to a reduced water vapor flux.[15] However, Figure 5a,b suggests that the water penetration in our membranes is marginal. In such a case, the flux enhancement caused by the increased liquid−air interfacial area would dominate.

Trade-off Between wetting Resistance and Water Vapor Flux is Absent in the Membrane Having Straight Cylindrical Pores. While we employed fibrous membranes in this study, the trade-off relation between wetting resistance and water vapor flux in DCMD has also been observed for microporous membranes fabricated by phase inversion (Figure 1). As illustrated in Figure 5, a fibrous or irregular pore structure is proposed to result in the increase in the liquid−air interfacial area when the liquid protrudes into membrane pores. If this is the case, we can anticipate that the trade-off relation would not be observed for membranes consisting of straight pores because the liquid−air interfacial areas would vary little even for different wetting resistances as long as pore wetting does not occur.

To validate this hypothesis, we employed anodized aluminum oxide (AAO) membranes that comprise cylindrical and straight nanopores with a nominal diameter of 200 nm (Figure 6a). The AAO membranes were hydrophobized by treating them with the four silane molecules (i.e., AS, FAS-3, FAS-9, and FAS-17). Like the QF membranes, the AAO

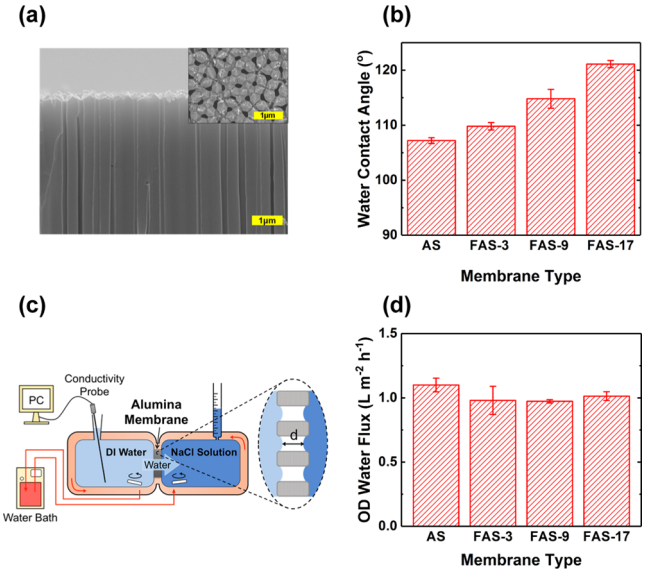

Figure 6. (a) Cross-sectional SEM micrograph of the pristine AAO membrane (the inset is the micrograph of the membrane surface). (b) Static contact angles of water on the surface of the AS, FAS-3, FAS-9, and FAS-17 AAO membranes. Error bars represent the standard deviations from three different membrane samples (both left and right contact angles were measured on each sample). (c) Schematic illustration of the osmotic distillation (OD) experimental setup. (d) OD water vapor fluxes of AS, FAS-3, FAS-9, and FAS-17 AAO membranes measured using distilled water at 40 °C as the feed solution and 4 M NaCl at 40 °C as the draw solution. Error bars represent the standard deviations.

membrane modified with the silane of a longer fluorocarbon chain was more hydrophobic (Figure 6b). The water vapor flux across the membranes was measured using a bench-scale OD setup (Figure 6c) used in our previous studies.[40,41] In the OD setup, the feed (distilled water) chamber and the draw (4 M NaCl solution) chamber were separated by the AAO membrane, which were both maintained at the same temperature (40 °C). In the OD process, the driving force of water vapor flow is the water vapor pressure gradient across the membrane created by the osmotic pressure difference between feed and draw. Therefore, OD can be considered as an isothermal variant of MD. The conductivity of feed (distilled water) remained constantly low for all tested membranes, without any occurrence of the membrane pore wetting. As shown in Figure 6d, the water vapor fluxes of AAO membranes modified with the four different silanes did not show significant differences (one-way ANOVA, $F = 3.14$, $p = 0.096$), and no trade-off relation between wetting resistance and water flux was observed. The results of OD experiments substantiate the impact of fibrous or irregular structures that allow liquid−air interfacial area expansion when the wetting resistance is lower.

Implications. In this study, we investigated the underlying mechanism for the wettability−flux trade-off relation in MD using quartz fiber (QF) membranes. We outline potential approaches for minimizing the impact of trade-off relation on attaining high water flux and their limitations. First, decreasing the thickness of a highly wetting-resistant membrane can be a feasible way to reduce the mass-transfer resistance of water vapor and thus offset the declined water flux. As previously shown, the penetration of liquid into the membrane pores was marginal even for the membrane having relatively high surface

https://dx.doi.org/10.1021/acs.est.0c02547
Environ. Sci. Technol. 2020, 54, 10333−10341

energy (e.g., AS QF membrane). Fabrication of composite membranes consisting of a thin hydrophobic porous layer on a thermally conductive supportive layer would increase the water flux for a given temperature difference.[48] It should be noted that water flux enhancement by reducing the membrane thickness would be limited by temperature polarization, in particular when the thickness becomes less than ~10 μm, and also be accompanied by a significant thermal conduction loss.[49,50]

Second, fabricating a membrane that comprises straight pores would not likely exhibit the trade-off relation. Many techniques for fabricating inorganic or polymeric membranes that have cylindrical pores have been explored, including electrochemical processes, selective etching of block copolymers, and imprinting.[51−53] However, fibrous or irregular pore structures are generally preferred for MD due to the high porosity and ease of membrane fabrication. Therefore, benefits from the membranes of straight pores with high wetting resistances may not be obvious for MD applications.

Third, the membrane surface energy can be tailored to obtain a high water vapor flux if the feed water of specific compositions is treated. The surface energy must be determined based on the minimum possible surface tension of the feed water. In such a case, a consistent minimum surface tension of the feed water needs to be guaranteed and a rigorous assessment for the risk of potential membrane wetting and the benefit of high water yield will be required.

■ ASSOCIATED CONTENT

Supporting Information

The Supporting Information is available free of charge at https://pubs.acs.org/doi/10.1021/acs.est.0c02547.

> Summary of the water flux data of the membrane before and after the surface modification in the literature and the water flux ratios, as well as the corresponding membrane characteristic changes calculated from the data in the literature; schematic illustration of hydrophobic modification processes; estimation of capacitance using EIS; membrane structure characterizations; measurement of water vapor flux and salt rejection in DCMD experiments; SEM micrographs of the morphologies of FAS-3 QF and FAS-9 QF membranes; characteristics of modified QF membranes; water vapor fluxes of the modified QF membranes in DCMD tests; impedance spectra of AS QF membrane; and estimated capacitances of the modified QF membranes based on the impedance measurements (PDF)

■ AUTHOR INFORMATION

Corresponding Authors

Xuesong Li − *State Key Laboratory of Pollution Control and Resource Reuse, Shanghai Institute of Pollution Control and Ecological Security, School of Environmental Science and Engineering, Tongji University, Shanghai 200092, China*; Phone: 86-21-65975669; Email: xuesong_li@tongji.edu.cn

Jongho Lee − *Department of Civil Engineering, University of British Columbia, Vancouver, British Columbia V6T 1Z4, Canada*; orcid.org/0000-0001-9602-2244; Phone: (604) 822-4694; Email: jongho.lee@civil.ubc.ca

Authors

Chenxi Li − *Department of Civil Engineering, University of British Columbia, Vancouver, British Columbia V6T 1Z4, Canada*

Xuewei Du − *Department of Civil and Environmental Engineering, Colorado State University, Fort Collins, Colorado 80526, United States*

Ying Zhang − *Department of Civil Engineering, University of British Columbia, Vancouver, British Columbia V6T 1Z4, Canada*

Wei Wang − *Department of Mechanical and Aerospace Engineering, North Carolina State University, Raleigh, North Carolina 27695, United States*; orcid.org/0000-0002-1260-2098

Tiezheng Tong − *Department of Civil and Environmental Engineering, Colorado State University, Fort Collins, Colorado 80526, United States*; orcid.org/0000-0002-9289-3330

Arun Kumar Kota − *Department of Mechanical and Aerospace Engineering, North Carolina State University, Raleigh, North Carolina 27695, United States*; orcid.org/0000-0001-9061-7896

Complete contact information is available at: https://pubs.acs.org/10.1021/acs.est.0c02547

Notes

The authors declare no competing financial interest.

■ ACKNOWLEDGMENTS

J.L. acknowledges funding support from the Natural Sciences and Engineering Research Council of Canada (NSERC) through the Discovery Grant. T.T acknowledges funding support from the Colorado Office of Economic Development and International Trade and CSU Ventures, as well as the Department of Civil and Environmental Engineering, College of Engineering at Colorado State University. A.K.K. acknowledges financial support under award 1751628 from the NSF and under awards R01HL135505 and R21HL139208 from the NIH.

■ REFERENCES

(1) World Water Assessment Programme (Wwap). *The United Nations World Water Development Report 4: Managing Water under Uncertainty and Risk*; UNESCO: Paris, 2012.

(2) Ranade, V. V.; Bhandari, V. M. Industrial Wastewater Treatment, Recycling, and Reuse: An Overview, In *Industrial Wastewater Treatment, Recycling and Reuse*, Ranade, V. V.; Bhandari, V. M., Eds.; Butterworth-Heinemann: Oxford, 2014; pp 1−80; Chapter 1.

(3) Tong, T.; Elimelech, M. The Global Rise of Zero Liquid Discharge for Wastewater Management: Drivers, Technologies, and Future Directions. *Environ. Sci. Technol.* **2016**, *50*, 6846−6855.

(4) Wwap (World Water Assessment Programme). *the United Nations World Water Development Report 2017: Wastewater—the Untapped Resource.*; UNESCO: Paris, 2017.

(5) Shaffer, D. L.; Arias Chavez, L. H.; Ben-Sasson, M.; Romero-Vargas Castrillón, S.; Yip, N. Y.; Elimelech, M. Desalination and Reuse of High-Salinity Shale Gas Produced Water: Drivers, Technologies, and Future Directions. *Environ. Sci. Technol.* **2013**, *47*, 9569−9583.

(6) Qasim, M.; Badrelzaman, M.; Darwish, N. N.; Darwish, N. A.; Hilal, N. Reverse Osmosis Desalination: A State-of-the-Art Review. *Desalination* **2019**, *459*, 59−104.

(7) Liao, Y.; Wang, R.; Fane, A. G. Engineering Superhydrophobic Surface on Poly(Vinylidene Fluoride) Nanofiber Membranes for Direct Contact Membrane Distillation. *J. Membr. Sci.* **2013**, *440*, 77−87.

(8) Boo, C.; Lee, J.; Elimelech, M. Omniphobic Polyvinylidene Fluoride (Pvdf) Membrane for Desalination of Shale Gas Produced Water by Membrane Distillation. *Environ. Sci. Technol.* **2016**, *50*, 12275−12282.
(9) Lee, J.; Boo, C.; Ryu, W.-H.; Taylor, A. D.; Elimelech, M. Development of Omniphobic Desalination Membranes Using a Charged Electrospun Nanofiber Scaffold. *ACS Appl. Mater. Interfaces* **2016**, *8*, 11154−11161.
(10) Du, X.; Zhang, Z.; Carlson, K. H.; Lee, J.; Tong, T. Membrane Fouling and Reusability in Membrane Distillation of Shale Oil and Gas Produced Water: Effects of Membrane Surface Wettability. *J. Membr. Sci.* **2018**, *567*, 199−208.
(11) Chew, N. G. P.; Zhao, S.; Malde, C.; Wang, R. Polyvinylidene Fluoride Membrane Modification Via Oxidant-Induced Dopamine Polymerization for Sustainable Direct-Contact Membrane Distillation. *J. Membr. Sci.* **2018**, *563*, 31−42.
(12) Mohammadi Ghaleni, M.; Al Balushi, A.; Kaviani, S.; Tavakoli, E.; Bavarian, M.; Nejati, S. Fabrication of Janus Membranes for Desalination of Oil-Contaminated Saline Water. *ACS Appl. Mater. Interfaces* **2018**, *10*, 44871−44879.
(13) Alkhudhiri, A.; Darwish, N.; Hilal, N. Membrane Distillation: A Comprehensive Review. *Desalination* **2012**, *287*, 2−18.
(14) Khayet, M. Membranes and Theoretical Modeling of Membrane Distillation: A Review. *Adv. Colloid Interface Sci.* **2011**, *164*, 56−88.
(15) Rezaei, M.; Warsinger, D. M.; Lienhard V, J. H.; Duke, M. C.; Matsuura, T.; Samhaber, W. M. Wetting Phenomena in Membrane Distillation: Mechanisms, Reversal, and Prevention. *Water Res.* **2018**, *139*, 329−352.
(16) Wang, Z.; Chen, Y.; Sun, X.; Duddu, R.; Lin, S. Mechanism of Pore Wetting in Membrane Distillation with Alcohol Vs. Surfactant. *J. Membr. Sci.* **2018**, *559*, 183−195.
(17) Lin, S.; Nejati, S.; Boo, C.; Hu, Y.; Osuji, C. O.; Elimelech, M. Omniphobic Membrane for Robust Membrane Distillation. *Environ. Sci. Technol. Lett.* **2014**, *1*, 443−447.
(18) Liu, T. L.; Kim, C.-J. C. Turning a Surface Superrepellent Even to Completely Wetting Liquids. *Science* **2014**, *346*, 1096−1100.
(19) Lu, K. J.; Zuo, J.; Chang, J.; Kuan, H. N.; Chung, T.-S. Omniphobic Hollow-Fiber Membranes for Vacuum Membrane Distillation. *Environ. Sci. Technol.* **2018**, *52*, 4472−4480.
(20) Li, C.; Li, X.; Du, X.; Tong, T.; Cath, T. Y.; Lee, J. Antiwetting and Antifouling Janus Membrane for Desalination of Saline Oily Wastewater by Membrane Distillation. *ACS Appl. Mater. Interfaces* **2019**, *11*, 18456−18465.
(21) McGaughey, A. L.; Karandikar, P.; Gupta, M.; Childress, A. E. Hydrophobicity Versus Pore Size: Polymer Coatings to Improve Membrane Wetting Resistance for Membrane Distillation. *ACS Appl. Polym. Mater.* **2020**, *2*, 1256−1267.
(22) Li, X.; Dutta, A.; Dong, Q.; Rollings-Scattergood, S.; Lee, J. Dissolved Methane Harvesting Using Omniphobic Membranes for Anaerobically Treated Wastewaters. *Environ. Sci. Technol. Lett.* **2019**, *6*, 228−234.
(23) Huang, Y. X.; Wang, Z.; Jin, J.; Lin, S. Novel Janus Membrane for Membrane Distillation with Simultaneous Fouling and Wetting Resistance. *Environ. Sci. Technol.* **2017**, *51*, 13304−13310.
(24) An, X.; Liu, Z.; Hu, Y. Amphiphobic Surface Modification of Electrospun Nanofibrous Membranes for Anti-Wetting Performance in Membrane Distillation. *Desalination* **2018**, *432*, 23−31.
(25) Lu, C.; Su, C.; Cao, H.; Ma, X.; Duan, F.; Chang, J.; Li, Y. F-Poss Based Omniphobic Membrane for Robust Membrane Distillation. *Mater. Lett.* **2018**, *228*, 85−88.
(26) Lu, X.; Peng, Y.; Qiu, H.; Liu, X.; Ge, L. Anti-Fouling Membranes by Manipulating Surface Wettability and Their Anti-Fouling Mechanism. *Desalination* **2017**, *413*, 127−135.
(27) Woo, Y. C.; Kim, Y.; Yao, M.; Tijing, L. D.; Choi, J. S.; Lee, S.; Kim, S. H.; Shon, H. K. Hierarchical Composite Membranes with Robust Omniphobic Surface Using Layer-by-Layer Assembly Technique. *Environ. Sci. Technol.* **2018**, *52*, 2186−2196.
(28) Zheng, R.; Chen, Y.; Wang, J.; Song, J.; Li, X.-M.; He, T. Preparation of Omniphobic Pvdf Membrane with Hierarchical Structure for Treating Saline Oily Wastewater Using Direct Contact Membrane Distillation. *J. Membr. Sci.* **2018**, *555*, 197−205.
(29) Wang, M.; Liu, G.; Yu, H.; Lee, S.-H.; Wang, L.; Zheng, J.; Wang, T.; Yun, Y.; Lee, J. K. Zno Nanorod Array Modified Pvdf Membrane with Superhydrophobic Surface for Vacuum Membrane Distillation Application. *ACS Appl. Mater. Interfaces* **2018**, *10*, 13452−13461.
(30) Karanikola, V.; Boo, C.; Rolf, J.; Elimelech, M. Engineered Slippery Surface to Mitigate Gypsum Scaling in Membrane Distillation for Treatment of Hypersaline Industrial Wastewaters. *Environ. Sci. Technol.* **2018**, *52*, 14362−14370.
(31) Wang, W.; Du, X.; Vahabi, H.; Zhao, S.; Yin, Y.; Kota, A. K.; Tong, T. Trade-Off in Membrane Distillation with Monolithic Omniphobic Membranes. *Nat. Commun.* **2019**, *10*, No. 3220.
(32) Chen, Y.; Lu, K. J.; Chung, T.-S. An Omniphobic Slippery Membrane with Simultaneous Anti-Wetting and Anti-Scaling Properties for Robust Membrane Distillation. *J. Membr. Sci.* **2020**, *595*, No. 117572.
(33) Chul Woo, Y.; Chen, Y.; Tijing, L. D.; Phuntsho, S.; He, T.; Choi, J.-S.; Kim, S.-H.; Kyong Shon, H. Cf4 Plasma-Modified Omniphobic Electrospun Nanofiber Membrane for Produced Water Brine Treatment by Membrane Distillation. *J. Membr. Sci.* **2017**, *529*, 234−242.
(34) Guo, J.; Deka, B. J.; Kim, K.-J.; An, A. K. Regeneration of Superhydrophobic Tio2 Electrospun Membranes in Seawater Desalination by Water Flushing in Membrane Distillation. *Desalination* **2019**, *468*, No. 114054.
(35) Chen, Y.; Tian, M.; Li, X.; Wang, Y.; An, A. K.; Fang, J.; He, T. Anti-Wetting Behavior of Negatively Charged Superhydrophobic Pvdf Membranes in Direct Contact Membrane Distillation of Emulsified Wastewaters. *J. Membr. Sci.* **2017**, *535*, 230−238.
(36) Palacio, L.; Prádanos, P.; Calvo, J. I.; Hernández, A. Porosity Measurements by a Gas Penetration Method and Other Techniques Applied to Membrane Characterization. *Thin Solid Films* **1999**, *348*, 22−29.
(37) Wu, S. Calculation of Interfacial Tension in Polymer Systems. *J. Polym. Sci., Polym. Symp.* **1971**, *34*, 19−30.
(38) Müller, M.; Oehr, C. Comments on "an Essay on Contact Angle Measurements" by Strobel and Lyons. *Plasma Process Polym.* **2011**, *8*, 19−24.
(39) Boo, C.; Lee, J.; Elimelech, M. Engineering Surface Energy and Nanostructure of Microporous Films for Expanded Membrane Distillation Applications. *Environ. Sci. Technol.* **2016**, *50*, 8112−8119.
(40) Lee, J.; Laoui, T.; Karnik, R. Nanofluidic Transport Governed by the Liquid/Vapour Interface. *Nat. Nanotechnol.* **2014**, *9*, 317−323.
(41) Lee, J.; Straub, A. P.; Elimelech, M. Vapor-Gap Membranes for Highly Selective Osmotically Driven Desalination. *J. Membr. Sci.* **2018**, *555*, 407−417.
(42) Chen, Y.; Wang, Z.; Jennings, G. K.; Lin, S. Probing Pore Wetting in Membrane Distillation Using Impedance: Early Detection and Mechanism of Surfactant-Induced Wetting. *Environ. Sci. Technol. Lett.* **2017**, *4*, 505−510.
(43) Huang, Q.; Luo, Q.; Chen, Z.; Yao, L.; Fu, P.; Lin, Z. The Effect of Electrolyte Concentration on Electrochemical Impedance for Evaluating Polysulfone Membranes. *Environ. Sci. Water Res. Technol.* **2018**, *4*, 1145−1151.
(44) Wang, D.; Dang, Z.-M. Processing of Polymeric Dielectrics for High Energy Density Capacitors, In *Dielectric Polymer Materials for High-Density Energy Storage*, Dang, Z.-M., Ed.; William Andrew Publishing, 2018; pp 429−446; Chapter 12.
(45) Matijević, E.; Pethica, B. A. The Properties of Ionized Monolayers. Part 1.—Sodium Dodecyl Sulphate at the Air/Water Interface. *Trans. Faraday Soc.* **1958**, *54*, 1382−1389.
(46) Tuteja, A.; Choi, W.; Ma, M. L.; Mabry, J. M.; Mazzella, S. A.; Rutledge, G. C.; McKinley, G. H.; Cohen, R. E. Designing Superoleophobic Surfaces. *Science* **2007**, *318*, 1618−1622.

https://dx.doi.org/10.1021/acs.est.0c02547
Environ. Sci. Technol. 2020, 54, 10333−10341

(47) Zhao, H.; Park, K.-C.; Law, K.-Y. Effect of Surface Texturing on Superoleophobicity, Contact Angle Hysteresis, and "Robustness". *Langmuir* **2012**, *28*, 14925−14934.
(48) Su, M.; Teoh, M. M.; Wang, K. Y.; Su, J.; Chung, T.-S. Effect of Inner-Layer Thermal Conductivity on Flux Enhancement of Dual-Layer Hollow Fiber Membranes in Direct Contact Membrane Distillation. *J. Membr. Sci.* **2010**, *364*, 278−289.
(49) Deshmukh, A.; Lee, J. Membrane Desalination Performance Governed by Molecular Reflection at the Liquid-Vapor Interface. *Int. J. Heat Mass Transfer* **2019**, *140*, 1006−1022.
(50) Drioli, E.; Ali, A.; Macedonio, F. Membrane Distillation: Recent Developments and Perspectives. *Desalination* **2015**, *356*, 56−84.
(51) Belwalkar, A.; Grasing, E.; Van Geertruyden, W.; Huang, Z.; Misiolek, W. Z. Effect of Processing Parameters on Pore Structure and Thickness of Anodic Aluminum Oxide (Aao) Tubular Membranes. *J. Membr. Sci.* **2008**, *319*, 192−198.
(52) Abetz, V. Isoporous Block Copolymer Membranes. *Macromol. Rapid Commun.* **2015**, *36*, 10−22.
(53) Zhan, Z.; Lei, Y. Sub-100-Nm Nanoparticle Arrays with Perfect Ordering and Tunable and Uniform Dimensions Fabricated by Combining Nanoimprinting with Ultrathin Alumina Membrane Technique. *ACS Nano* **2014**, *8*, 3862−3868.

https://dx.doi.org/10.1021/acs.est.0c02547
Environ. Sci. Technol. 2020, 54, 10333−10341